Journal of Computational Physics 227 (2008) 8655–8671

Contents lists available at ScienceDirect

Journal of Computational Physics

journal homepage: www.elsevier.com/locate/jcp

# Accuracy of higher-order lattice Boltzmann methods for microscale flows with finite Knudsen numbers

Seung Hyun Kim [a,*], Heinz Pitsch [a], Iain D. Boyd [b]

[a] Department of Mechanical Engineering, Stanford University, Stanford, CA 94305-3035, United States
[b] Department of Aerospace Engineering, University of Michigan, MI 48109-2140, United States

ARTICLE INFO

*Article history:*
Received 22 October 2007
Received in revised form 23 April 2008
Accepted 16 June 2008
Available online 25 June 2008

*Keywords:*
Lattice Boltzmann method
Kinetic theory
Microscale flow

ABSTRACT

Accuracy of the lattice Boltzmann (LB) method for microscale flows with finite Knudsen numbers is investigated. We employ up to the eleventh-order Gauss–Hermite quadrature for the lattice velocities and diffuse-scattering boundary condition for fluid–wall interactions. Detailed comparisons with the direct simulation Monte Carlo (DSMC) method and the linearized Boltzmann equation are made for planar Couette and Poiseuille flows. All higher-order LB methods considered here give improved results as compared with the standard LB method. The accuracy of the LB hierarchy, however, does not monotonically increase with the order of the Gauss–Hermite quadrature at moderate and large Knudsen numbers. The results also show the sensitivity to a quadrature chosen, even when the Gauss–Hermite quadratures have the same order of formal accuracy. Among the schemes investigated here, D2Q16 is the most efficient method and offers a quantitative prediction in the slip and transition regimes. The higher-order LB methods predict the Knudsen layer up to $Kn = O(0.1)$. The Knudsen layer, however, rapidly disappears when the Knudsen number approaches unity due to a finite number of the lattice velocities, while it is still present for $Kn = O(1)$ in the Boltzmann equation. It is also found that the higher-order LB methods adopted here do not capture the asymptotic behavior of the Boltzmann equation at large Knudsen numbers.



## 1. Introduction

Fluid flows in small-scale confined geometry has recently attracted significant attention due to the advancement of micro and nanotechnology [1,2]. The flow in this regime is characterized by the Knudsen number, $Kn = \lambda/H$, where $\lambda$ is the mean free path of molecules and $H$ is the characteristic length scale of the geometry [2,3]. At very small Kn, the kinetic theory predicts that hydrodynamics in a homogeneous bulk fluid is described by the Navier–Stokes equations [4,5]. However, for finite $Kn$ flows, the no-slip boundary condition for fluid–wall interactions, which prevails in the continuum hydrodynamic simulations, breaks down, because of the increasing importance of the presence of the Knudsen layer [2]. The Navier–Stokes equations can also break down at even higher $Kn$.

Hydrodynamics beyond the Navier–Stokes equations can be described by the Boltzmann equation [5]. The Boltzmann equation is an integro-differential equation with $2D + 1$ independent variables for a system with $D$-dimensions in physical space. Due to the large dimensionality and complexity in the collision operator, analytic solutions of the Boltzmann equation are limited to simple flows. The direct simulation Monte Carlo (DSMC) method [6] is a stochastic numerical method to solve the Boltzmann equation [7]. The large dimensionality in the Boltzmann equation makes DSMC efficient, since the

* Corresponding author.
*E-mail address:* shkcomb@stanford.edu (S.H. Kim).

0021-9991/$ - see front matter © 2008 Elsevier Inc. All rights reserved.
doi:10.1016/j.jcp.2008.06.012

convergence of the Monte Carlo method only depends on the number of stochastic particles. However, the application of DSMC to engineering problems is limited, due to the relatively high computational cost, especially for low-speed flows.

The lattice Boltzmann (LB) method [8–12] is a reduced-order model of the Boltzmann equation. While originated from lattice-gas automata (LGA) [10], the LB method with a single relaxation time Bhatnagar–Gross–Krook (BGK) collision operator has been proven to be a special discrete form of the corresponding Boltzmann equation [13,14]. The discretization in velocity space is made by using the Gauss–Hermite quadrature such that the lower moments of single-particle distribution functions obey the Navier–Stokes equations [13,14]. While the LB method is originally designed to mimic the Navier–Stokes hydrodynamics, due to its kinetic origin, a number of studies have been reported for application of the LB method in finite *Kn* flows with encouraging results [15–23]. In earlier work, attention has been devoted primarily to fluid–wall interactions, in order to reproduce the slip phenomena [17,23]. Among others, the diffuse-scattering boundary condition is shown to well reproduce the slip phenomena for $Kn < 0.1$ [17,20,21]. For higher *Kn* flows, a modification to relaxation dynamics, such as "virtual wall collision" [18], has also been proposed. Although encouraging results have been reported, there has also been criticism for application of the LB method to finite *Kn* flows. Traditionally, the LB method is a second-order scheme in the Chapman–Enskog expansion [10]. This has led to the viewpoint that the LB method cannot be applied to finite *Kn* flows, due to the lack of the physical symmetry and spatial accuracy [24,25].

The multi-speed or higher-order LB models have been developed to increase the order of accuracy in the discretization of velocity phase space. A systematic derivation of the LB equation for higher-order hydrodynamics has been presented in Shan and He [14] and Shan et al. [26]. In their approach, the higher-order LB equation is obtained from the systematic approximation of the Boltzmann equation using the Hermite basis in velocity space, or equivalently Gauss–Hermite quadratures, and the spatial and time discretization of the resulting discrete velocity Boltzmann equation. The connection between the Grad's moment system and the discrete velocity model has been utilized to construct the discrete velocity equilibrium function embodying the *H*-theorem in discrete phase space [27,28]. The quadrature sets with the speed of discrete velocities being integer multiples of the smallest speed in the same direction have also been developed [26,29,30], where the so-called propagation/collision dynamics can be applied. Ansumali et al. [31] presented analytical solutions of the discrete velocity Boltzmann equation for Couette flow using the so-called D2Q9 and D2Q16 schemes and showed that the increase of order in the Gauss–Hermite quadrature results in a much more accurate treatment of finite *Kn* flows. However, no systematic study on the quadrature set higher than D2Q16 has been reported.

In this paper, we present a systematic study on the accuracy of the LB hierarchy for finite *Kn* flows. The discrete velocity-sets for up to the eleventh-order Gauss–Hermite quadrature are employed, and detailed comparisons with reference solutions are made for the canonical problems for microscale flows, planar Couette and Poiseuille flows. In Section 2, the derivation of the LB equation from the Boltzmann equation with the BGK collision operator is presented. Discretization, non-dimensionalization, and relationship of the relaxation time and the Knudsen number are discussed in the context of the consistency with the continuum kinetic theory. The kinetic boundary condition for the higher-order LB method is also described. In Section 3, the higher-order LB methods are validated against DSMC and the linearized Boltzmann equation with emphasis on convergence and accuracy at small and moderate *Kn*, the Knudsen layer, and the asymptotic behavior at large *Kn*. A summary of the major conclusions is presented in Section 4.

## 2. Lattice Boltzmann method

### 2.1. Boltzmann–BGK equation

The Boltzmann equation with a single relaxation time BGK collision operator can be written as

$$\frac{\partial f}{\partial t} + \mathbf{c}\cdot\nabla f + \mathbf{g}\cdot\nabla_{\mathbf{c}} f = -\frac{1}{\tau}(f - f^{\mathrm{eq}}), \tag{1}$$

where $f(\mathbf{x},\mathbf{c},t)$ is the single-particle distribution at a location $\mathbf{x}$ with velocity $\mathbf{c}$ at time $t$, $\tau$ is the relaxation time, and $\mathbf{g}$ is an external force. The local equilibrium distribution $f^{\mathrm{eq}}$ is given by

$$f^{\mathrm{eq}} = \rho\left(\frac{m}{2\pi k_B T}\right)^{D/2} \exp\left(-\frac{m|\mathbf{c}-\mathbf{u}|^2}{2k_B T}\right), \tag{2}$$

where $m$ is the mass of the fluid particle, and $k_B$ is the Boltzmann constant. The density, fluid velocity, and temperature are, respectively, given by

$$\rho = \int f \mathrm{d}\mathbf{c} \tag{3}$$

$$\rho\mathbf{u} = \int \mathbf{c} f \mathrm{d}\mathbf{c} \tag{4}$$

$$\frac{D}{2}\rho RT = \int |\mathbf{c}-\mathbf{u}|^2 f \mathrm{d}\mathbf{c}. \tag{5}$$

Using the Chapman–Enskog expansion, the kinematic viscosity is obtained as

$$\nu = \tau c_s^2, \tag{6}$$

where $c_s = \sqrt{k_B T/m}$ is the speed of sound. Here we are interested in isothermal flow, and the temperature $T$ is assumed constant. The equation of state is $p = c_s^2 \rho$, where $p$ is the pressure.

### 2.2. Discretization in velocity space

In a discrete velocity version of the Boltzmann equation, the system is described by a finite set of (weighted) distribution functions for discrete velocities evolving in $(\mathbf{x}, t)$ space. To recover the hydrodynamic equations at the Navier–Stokes or higher level, the lower-order moments, Eqs. (3) and (4), and the corresponding fluxes are to be evaluated exactly using the distribution functions for the discrete velocities, and a proper form of the discrete equilibrium distribution function is to be derived. Here we follow the moment expansion approach of Shan and He [14] and Shan et al. [26] to derive the equilibrium distribution function and the evolution equation.

In the moment expansion approach, the discretization in velocity space is done by projecting the distribution function onto a functional space spanned by the orthogonal Hermite basis:

$$f(\mathbf{c}, \mathbf{x}, t) \approx f^N(\mathbf{c}, \mathbf{x}, t) = \omega(\mathbf{c}) \sum_{n=0}^{N} \frac{1}{n!} a^{(n)}(\mathbf{x}, t) H^{(n)}(\mathbf{c}), \tag{7}$$

where $H^{(n)}$ is the $n$th order Hermite polynomial. The weight function $\omega(\mathbf{c})$ is given by

$$\omega(\mathbf{c}) = \frac{\bar{\omega}(\mathbf{q})}{c_s^D} = \frac{1}{c_s^D} \frac{1}{(2\pi)^{D/2}} \exp\left(-\frac{|\mathbf{q}|^2}{2}\right), \tag{8}$$

where $\mathbf{q} = \mathbf{c}/c_s$. The coefficients $a^{(n)}$ are given by

$$a^{(n)} = \int f^N H^{(n)} \mathrm{d}\mathbf{c} = \int \omega \frac{f^N}{\omega} H^{(n)} \mathrm{d}\mathbf{c}. \tag{9}$$

Hermite polynomials are useful in constructing a reduced-order model for the Boltzmann equation, because the coefficients $a^{(n)}$ correspond to the moments of the distribution functions [26]. Considering that $f^N H^{(n)}/\omega$ is a polynomial of order $\leqslant 2N$ (in velocity space), the integral in Eq. (10) can be evaluated exactly with the $2N$-th order Gauss–Hermite quadrature or higher [32]:

$$a^{(n)} = \sum_{i=1}^{d} \frac{w_i f(\mathbf{c}_i) H^{(n)}(\mathbf{c}_i)}{\omega(\mathbf{c}_i)}. \tag{10}$$

Here, the discrete velocities $\mathbf{c}_i$ are given by $c_s \mathbf{q}_i$, where $\mathbf{q}_i$ are quadrature points for a Gauss–Hermite quadrature with respect to the weight function $\bar{\omega}(\mathbf{q})$. $w_i$ is the weight function for $\mathbf{q}_i$, and $d$ is the number of quadrature points. Since the evaluation of the integral in Eq. (10) requires values of $f$ for only the discrete velocities, $\mathbf{c}_i$, the approximation using the Hermite basis, i.e. obtaining the Hermite coefficients $a^{(n)}$, is equivalent to solving the set of distribution functions at the discrete velocities (Gauss–Hermite quadrature points) [14]. In Eq. (10), a coefficient of the Hermite expansion is a linear function of hydrodynamic moments [26]. The conserved moments, the fluid density $\rho$ and the momentum density $\rho\mathbf{u} = \rho(u, v, w)^{\mathrm{T}}$, are given by

$$\sum f_i = \rho \tag{11}$$

$$\sum \mathbf{c}_i f_i = \rho \mathbf{u}, \tag{12}$$

where $f_i = w_i f(\mathbf{c}_i)/\omega(\mathbf{c}_i)$.

The discrete velocity Boltzmann–BGK equation can be derived by projecting the Boltzmann equation onto the finite functional space represented by the Hermite basis:

$$\frac{\partial f_i}{\partial t} + \mathbf{c}_i \cdot \nabla f_i = -\frac{1}{\tau}(f_i - f_i^{\mathrm{eq}}) + F_i = \Omega_i + F_i, \tag{13}$$

where $F_i$ is an external force for the velocity $\mathbf{c}_i$. Depending on the truncation order, $\Omega_i$ and $F_i$ can have higher-order moments terms. Here, of primary interest are low Mach number ($Ma$) flows, and terms up to second-order are retained in the Hermite expansion [26]:

$$f_i^{\mathrm{eq}} = w_i \rho \left[1 + \frac{\mathbf{u} \cdot \mathbf{c}_i}{c_s^2} + \frac{1}{2}\frac{(\mathbf{u} \cdot \mathbf{c}_i)^2}{c_s^4} - \frac{1}{2}\frac{(\mathbf{u} \cdot \mathbf{u})}{c_s^2}\right], \tag{14}$$

$$F_i = w_i \rho \left[\frac{\mathbf{g} \cdot \mathbf{c}_i}{c_s^2} + \frac{(\mathbf{g} \cdot \mathbf{c}_i)(\mathbf{u} \cdot \mathbf{c}_i)}{c_s^4} - \frac{\mathbf{g} \cdot \mathbf{u}}{c_s^2}\right]. \tag{15}$$

In Eq. (7), the order in the Hermite expansion determines the accuracy of the velocity space discretization. To recover the athermal Navier–Stokes equations, second-order terms should be retained. While we employ only up to the second-order moment terms in the discrete equilibrium and forcing terms for low-speed flows, the accuracy of the velocity space discretization can be improved by adopting a higher-order Gauss–Hermite quadrature. Table 1 shows 1D Gauss–Hermite quadratures for the 5th–11th order. A 2D quadrature can be obtained from the product of the corresponding 1D quadrature [26]. For example, the conventional D2Q9 scheme is a production formula of D1Q3. For the D2Q9 scheme [12], the discrete velocities are thus given as

$$\mathbf{c}_i = \begin{cases} (0,0), & \text{for } i = 0 \\ \sqrt{3}c_s(\cos[(i-1)\pi/2], \sin[(i-1)\pi/2]), & \text{for } i = 1,2,3,4 \\ \sqrt{3}c_s(\sqrt{2}\cos[(2i-9)\pi/4], \sqrt{2}\sin[(2i-9)\pi/4]), & \text{for } i = 5,6,7,8. \end{cases} \tag{16}$$

The weights are $w_0 = 4/9$, $w_1 = w_2 = w_3 = w_4 = 1/9$, and $w_5 = w_6 = w_7 = w_8 = 1/36$. Table 2 shows two Gauss–Hermite quadratures exclusively designed for 2D problems. Both of these and the D2Q16 scheme are of seventh-order accuracy, and correspond to the next member of the LB hierarchy over the standard quadrature D2Q9. An important feature of the D2Q21 scheme is that the discrete velocities are multiple integers of the velocities with the smallest speed. The propagation/collision dynamics can therefore be applied for D2Q21. The D2Q12 scheme has the smallest number of discrete velocities in the quadrature sets with seventh-order accuracy.

### 2.3. Lattice Boltzmann equation: time and spatial discretization, and non-dimensionalization

The LB equation can be obtained by discretizing the discrete velocity Boltzmann–BGK equation in time $t$ and space $\mathbf{x}$. By integrating Eq. (13) along the trajectory of the particle velocity $\mathbf{c}_i$ [13], we obtain

$$f_i(\mathbf{x} + \delta t\mathbf{c}_i, t + \delta t) - f_i(\mathbf{x}, t) = \int_0^{\delta t} \Omega_i(\mathbf{x} + t'\mathbf{c}_i, t + t')\mathrm{d}t' + F_i\delta t. \tag{17}$$

The integral in Eq. (17) can be approximated by

$$\int_0^{\delta t} \Omega_i(\mathbf{x} + t'\mathbf{c}_i, t + t')\mathrm{d}t' \approx \frac{\delta t}{2}[\Omega_i(\mathbf{x} + \delta t\mathbf{c}_i, t + \delta t) + \Omega_i(\mathbf{x}, t)] + \mathrm{O}(\delta t^3). \tag{18}$$

**Table 1**
1D Gauss–Hermite quadratures of 5th–11th order accuracy

| Quadrature | Order | $q_i$ | $w_i$ |
|---|---|---|---|
| D1Q3 | 5 | 0 | 2/3 |
| | | $\pm\sqrt{3}$ | 1/6 |
| D1Q4 | 7 | $\pm\sqrt{3-\sqrt{6}}$ | $(3+\sqrt{6})/12$ |
| | | $\pm\sqrt{3+\sqrt{6}}$ | $(3-\sqrt{6})/12$ |
| D1Q5 | 9 | 0 | 8/15 |
| | | $\pm\sqrt{5-\sqrt{10}}$ | $(7+2\sqrt{10})/60$ |
| | | $\pm\sqrt{5+\sqrt{10}}$ | $(7-2\sqrt{10})/60$ |
| D1Q6 | 11 | ±0.616706590193136 | $4.08828469555808 \times 10^{-1}$ |
| | | ±1.88917587775414 | $8.861574604199542 \times 10^{-2}$ |
| | | ±3.32425743355142 | $2.555784402056898 \times 10^{-3}$ |

$q_i$ and $w_i$ are quadrature points and weights, respectively.

**Table 2**
Seventh-order 2D Gauss–Hermite quadratures

| Quadrature | $p$ | $\mathbf{q}_i$ | $w_i$ | |
|---|---|---|---|---|
| D2Q12 | 4 | $(\pm r, \pm r)$ | $(5+2\sqrt{5})/45$ | $r^2 = (9-3\sqrt{5})/4$ |
| | 4 | $(\pm s, \pm s)$ | $(5-2\sqrt{5})/45$ | $s^2 = (9+3\sqrt{5})/4$ |
| | 4 | $(t,0)_{FS}$ | 1/36 | $t^2 = 6$ |
| D2Q21 | 1 | (0,0) | 91/324 | $r^2 = 3/2$ |
| | 4 | $(r,0)_{FS}$ | 1/12 | |
| | 4 | $(\pm r, \pm r)$ | 2/27 | |
| | 4 | $(2r,0)_{FS}$ | 7/360 | |
| | 4 | $(\pm 2r, \pm 2r)$ | 1/432 | |
| | 4 | $(3r,0)_{FS}$ | 1/1620 | |

$\mathbf{q}_i$ are quadrature points, $w_i$ are weights, and $p$ is the number of velocities with the same speed. The subscript, *FS*, denotes a fully symmetric set of points. In D2Q21 [26], the discrete velocities are multiple integers of the velocities with the smallest speed. The D2Q12 scheme [32] has the smallest number of discrete velocities in the quadrature sets with seventh-order accuracy.

By introducing the transformation $\hat{f} = f - \delta t/2\Omega_i$ [33], the LB equation can be written as

$$\hat{f}_i(\mathbf{x} + \delta t\mathbf{c}_i, t + \delta t) - \hat{f}_i(\mathbf{x}, t) = -\frac{\delta t}{\tau + \delta t/2}\left(\hat{f}_i - f_i^{(0)}\right) + F_i\delta t. \tag{19}$$

This solves the discrete Boltzmann–BGK equation with second-order in $\delta t$ except for the forcing term which is of first-order. By increasing the order of the Gauss–Hermite quadrature, i.e. the order in the Hermite expansion, and decreasing the time step $\delta t$, the LB equation converges to the Boltzmann–BGK equation.

Eq. (19) is scaled with the time scale $t_0$ and the length scale $x_0 = c_s t_0/a$, where $a$ is a non-dimensional constant that is used here to represent different ways of non-dimensionalization. From this we obtain

$$\bar{f}_i(\bar{\mathbf{x}} + \delta\bar{t}\bar{\mathbf{c}}_i, \bar{t} + \delta\bar{t}) - \bar{f}_i(\bar{\mathbf{x}}, \bar{t}) = -\frac{\delta\bar{t}}{\bar{\tau} + \delta\bar{t}/2}\left(\bar{f}_i - \bar{f}_i^{\mathrm{eq}}\right) + \bar{F}_i\delta\bar{t}, \tag{20}$$

where the equilibrium distribution $f_i^{\mathrm{eq}}$ is given by

$$\bar{f}_i^{\mathrm{eq}} = w_i\bar{\rho}\left[1 + \frac{\bar{\mathbf{u}}\cdot\bar{\mathbf{c}}_i}{a^2} + \frac{1}{2}\frac{(\bar{\mathbf{u}}\cdot\bar{\mathbf{c}}_i)^2}{a^4} - \frac{1}{2}\frac{(\bar{\mathbf{u}}\cdot\bar{\mathbf{u}})}{a^2}\right]. \tag{21}$$

The overline denotes a quantity in the scaled unit. The mass $m_0$ can be appropriately chosen such that the density in the scaled unit is of order unity. The discrete velocity in the scaled unit is $\bar{\mathbf{c}}_i = a/c_s\mathbf{c}_i$. It is noted that $a$ is the sound speed in the non-dimensionalized equation. The non-dimensional sound speed $a$ can be chosen arbitrarily. To preserve the so-called propagation/collision dynamics in the standard LB method, the lattice spacing is chosen as $\delta = \delta\bar{t}\bar{c}_0$, where $c_0$ is a non-trivial component of the particle velocity, e.g. $\sqrt{3}c_s$ for D2Q9. The length of the computational domain is then $N\delta\bar{t}\bar{c}_0$, where $N$ is the number of lattice points in one coordinate. Traditionally, in the LB method, the lattice spacing $\delta$ and the time $\delta\bar{t}$ are set to unity. The length scale $x_0$ is then equal to the lattice spacing $\delta$, and the total length is given as $N$. This gives $a = 1/\sqrt{3}$ in D2Q9. Alternatively, in Shan et al. [26], the non-dimensional sound speed $a$ is set to unity, while the particle speed $\bar{c}_0$ is usually set to unity in the standard LB formulation. With this scaling, the lattice spacing $\delta$ is generally not the same as the length scale $x_0$, and the total length is not equal to $N$ when $c_0 \neq c_s$. For D2Q9, with this sound speed scaling, the total length of the computation domain is $\sqrt{3}N$. Hereafter, the overline for the scaled quantity is omitted for clarity.

In multi-speed LB methods, such as D2Q16, since all quadrature points do not coincide with the lattice points, the propagation/collision dynamics are not applicable. While several approaches have been proposed to apply the LB method in the non-lattice grid system, the finite difference method [34] is employed here. Applying the forward Euler method for time discretization and the second-order total variation diminishing (TVD) scheme for spatial discretization along the characteristic line, we obtain

$$f_i(\mathbf{x}, t + \delta_t) = f_i(\mathbf{x}, t) + \delta_t\frac{|\mathbf{c}_{ix}|}{\delta_x}\left[f_i\left(\mathbf{x} + \frac{\mathbf{c}_i}{|\mathbf{c}_{ix}|}\frac{\delta_x}{2}, t\right) - f_i\left(\mathbf{x} - \frac{\mathbf{c}_i}{|\mathbf{c}_{ix}|}\frac{\delta_x}{2}, t\right)\right] + \Omega_i\delta_t + F_i\delta_t, \tag{22}$$

where $\delta_t$ and $\delta_x$ are the time step and the (uniform) grid spacing, respectively. $\mathbf{c}_{i\alpha}$ is $(\mathbf{c}_i\cdot\mathbf{e}_\alpha)\mathbf{e}_\alpha$, where $\mathbf{e}_\alpha$ is the unit vector in the $\alpha$ direction. The face values are given by

$$f_i\left(\mathbf{x} + \frac{\mathbf{c}_i}{|\mathbf{c}_{ix}|}\frac{\delta_x}{2}, t\right) = \phi_i^L\left(\mathbf{x} + \frac{\mathbf{c}_i}{|\mathbf{c}_{ix}|}\frac{\delta_x}{2}, t\right) + \psi\left[\phi_i^H\left(\mathbf{x} + \frac{\mathbf{c}_i}{|\mathbf{c}_{ix}|}\frac{\delta_x}{2}, t\right) - \phi_i^L\left(\mathbf{x} + \frac{\mathbf{c}_i}{|\mathbf{c}_{ix}|}\frac{\delta_x}{2}, t\right)\right]. \tag{23}$$

The lower-order flux $\phi_L$ and the higher-order flux $\phi_H$ can be given by

$$\phi_i^L\left(\mathbf{x} + \frac{\mathbf{c}_i}{|\mathbf{c}_{ix}|}\frac{\delta_x}{2}, t\right) = f_i(\mathbf{x}, t) \tag{24}$$

$$\phi_i^H\left(\mathbf{x} + \frac{\mathbf{c}_i}{|\mathbf{c}_{ix}|}\frac{\delta_x}{2}, t\right) = \frac{f_i(\mathbf{x} + \mathbf{c}_i/|\mathbf{c}_{ix}|\delta_x, t) + f_i(\mathbf{x}, t)}{2}. \tag{25}$$

The flux limiter $\psi$ is chosen such that the scheme is globally of second-order and TVD. The MUSCL scheme of van Leer [35] is used here for the flux limiter:

$$\psi(r) = \max\left[0, \min\left(2r, \frac{r+1}{2}, 2\right)\right], \tag{26}$$

where

$$r = \frac{f_i(\mathbf{x}, t) - f_i(\mathbf{x} - \mathbf{c}_i/|\mathbf{c}_{ix}|\delta_x, t)}{f_i(\mathbf{x} + \mathbf{c}_i/|\mathbf{c}_{ix}|\delta_x, t) - f_i(\mathbf{x}, t)}. \tag{27}$$

When the grid points do not align with the characteristic line, the discrete equation is given by

$$f_i(\mathbf{x}, t+\delta_t) = f_i(\mathbf{x}, t) + \Omega_i \delta_t + F_i \delta_t + \delta_t \frac{|\mathbf{c}_{ix}|}{\delta_x}\left[f_i\left(\mathbf{x} + \frac{\mathbf{c}_{ix}}{|\mathbf{c}_{ix}|}\frac{\delta_x}{2}, t\right) - f_i\left(\mathbf{x} - \frac{\mathbf{c}_{ix}}{|\mathbf{c}_{ix}|}\frac{\delta_x}{2}, t\right)\right] + \delta_t \frac{|\mathbf{c}_{iy}|}{\delta_x}\left[f_i\left(\mathbf{x} + \frac{\mathbf{c}_{iy}}{|\mathbf{c}_{iy}|}\frac{\delta_x}{2}, t\right) - f_i\left(\mathbf{x} - \frac{\mathbf{c}_{iy}}{|\mathbf{c}_{iy}|}\frac{\delta_x}{2}, t\right)\right]. \tag{28}$$

Here, the accuracy of discretization in velocity phase space is investigated in steady flows. A recently developed off-lattice discretization method [36,37] can be used for improved stability and time accuracy.

### 2.4. Relaxation time and Knudsen number

In simulations of microscale flows, the relationship of the relaxation time $\tau$ and the mean free path $\lambda$ should be provided in the LB method with the BGK collision operator. The relationship of $\tau$ and $\lambda$ in the LB method was firstly presented in Nie et al. [15]. In the literature for the LB method, the relationship of $\tau$ and $\lambda$ and the definition of $Kn$ are, however, diverse [15,16,20,38,25,39,18]. Since the LB method converges to the continuum Boltzmann–BGK equation for $\delta t \to 0$ and $N \to \infty$, the mean free path for the LB method is chosen to be that for the Boltzmann–BGK equation here.

The mean free path $\lambda$ is an average distance travelled by a molecule before colliding with another molecule. In hard sphere gases it is well-defined and an exact expression can be obtained [4]. However, because collisions due to the intermolecular interaction are well-defined only for hard sphere molecules [5,2], the mean free path remains a conceptual quantity in general [40]. In that sense, the mean free path for the BGK molecules and thus for the LB method can be chosen arbitrarily, provided that it estimates the length scale of the molecular collision.

In the description of experiments or theoretical studies, the Knudsen number is typically defined using the viscosity, following the idea of Cercignani [5]:

$$\lambda_v = \frac{\mu}{p}\sqrt{\frac{\pi m k_B T}{2}} = \sqrt{\frac{\pi}{2}}\frac{v}{c_s}. \tag{29}$$

The viscosity-based mean free path $\lambda_v$ is very close to the exact result for hard sphere molecules, and thus provides a good estimate of the length scale of the molecular collision even for molecules other than hard sphere ones. This choice is also particularly attractive for the BGK molecules, since the relaxation time $\tau$ in the Boltzmann–BGK equation is determined to match the viscosity of the bulk fluid. Using the viscosity-based mean free path, Eq. (29), the mean free path for the BGK molecules can be defined as

$$\lambda = \sqrt{\frac{\pi}{2}}\frac{v}{c_s} = \sqrt{\frac{\pi}{2}}\tau c_s. \tag{30}$$

The Knudsen number is thus given by

$$Kn = \frac{\lambda}{H} = \sqrt{\frac{\pi}{2}}\frac{v}{c_s H}. \tag{31}$$

This is the relationship of the relaxation time and $Kn$ adopted here for the LB method [41].

For the validation of the LB method for microscale flows, the definition of $Kn$ in the LB method should be equivalent to that in the description of reference solutions including experimental measurements. This consistency in the definition of $Kn$ is often neglected in the LB literature [15,16,20].

### 2.5. Kinetic boundary condition

In the kinetic theory, a wall boundary condition [42] is given by

$$|(\mathbf{c} - \mathbf{u}_w)\cdot\mathbf{n}| f(\mathbf{c}, \mathbf{x}_w, t) = \int_{(\mathbf{c}'-\mathbf{u}_w)\cdot\mathbf{n}<0} |(\mathbf{c}' - \mathbf{u}_w)\cdot\mathbf{n}| f(\mathbf{c}', \mathbf{x}_w, t) R(\xi' \to \xi) \mathrm{d}\xi', \tag{32}$$

where the subscript $w$ denotes a quantity on the wall, $\mathbf{n}$ is the inward wall-normal vector, and $\xi = \mathbf{c} - \mathbf{u}_w$. $R(\xi' \to \xi)\mathrm{d}\xi$ is the probability of finding particles with velocities between $\xi$ and $\xi + \mathrm{d}\xi$ scattered from impinging particles with velocity $\xi'$. It is assumed in Eq. (32) that impinging particles are scattered with no time delay. With no mass flux across the wall, the scattering kernel $R$ satisfies

$$\int_{\xi'\cdot\mathbf{n}<0} R(\xi' \to \xi)\mathrm{d}\xi' = 1. \tag{33}$$

Another condition that $R$ satisfies is the detailed balance condition [42]:

$$|(\mathbf{c}' - \mathbf{u}_w)\cdot\mathbf{n}| f^{\mathrm{eq}}(\mathbf{c}', t) R(\xi' \to \xi) = |(\mathbf{c} - \mathbf{u}_w)\cdot\mathbf{n}| f^{\mathrm{eq}}(\mathbf{c}, t) R(-\xi \to -\xi'). \tag{34}$$

The discrete form of the kinetic boundary condition for the diffuse-scattering kernel [17], derived from Eq. (32), can be written as

$$f_i(\mathbf{x}_w, t) = \Psi f_i^{eq}(\rho_w, \mathbf{u}_w), \tag{35}$$

where

$$\Psi = \frac{\sum_{(\mathbf{c}_j - \mathbf{u}_w)<0} |(\mathbf{c}_j - \mathbf{u}_w)\cdot \mathbf{n}| f_j}{\sum_{(\mathbf{c}_k - \mathbf{u}_w)>0} |(\mathbf{c}_k - \mathbf{u}_w)\cdot \mathbf{n}| f_k^{eq}}. \tag{36}$$

In steady unidirectional flows, Eq. (35) reduces to (see Appendix)

$$f_i(\mathbf{x}_w, t) = f_i^{eq}(\rho_w, \mathbf{u}_w). \tag{37}$$

Other forms of the diffuse-scattering boundary condition can be found in Sofonea and Sekerka [21].

For the propagation/collision dynamics of D2Q21, some particles move two or three lattices at each time step. For these particles, if they are leaving a wall boundary, the distribution functions for lattices between the wall boundary lattice and the lattice where the particles arrive after $\delta t$, is set to be the distribution functions at the corresponding values at the boundary lattice. For example, the particles with the lattice velocity $(3r, 0)$ move three lattices in a propagation step. After a propagation step, $f$ at $\mathbf{x}_w + (r, 0)$ and $\mathbf{x}_w + (2r, 0)$ are set to $f$ at $\mathbf{x}_w + (3r, 0)$. The location of the wall boundary is the same as for the half-way bounce-back scheme [21,43]. When the wall boundary is located at $y = 0$, where $y$ is the direction normal to the wall, a layer of the wall boundary lattices is located at $y = -1/2\delta x$ [21,43]. For the finite difference LB method, the collision term is not closed for lattices at the wall boundary. To evaluate the equilibrium distribution at the wall, the density can be extrapolated from the interior lattices. For the problems investigated here, the density is uniform.

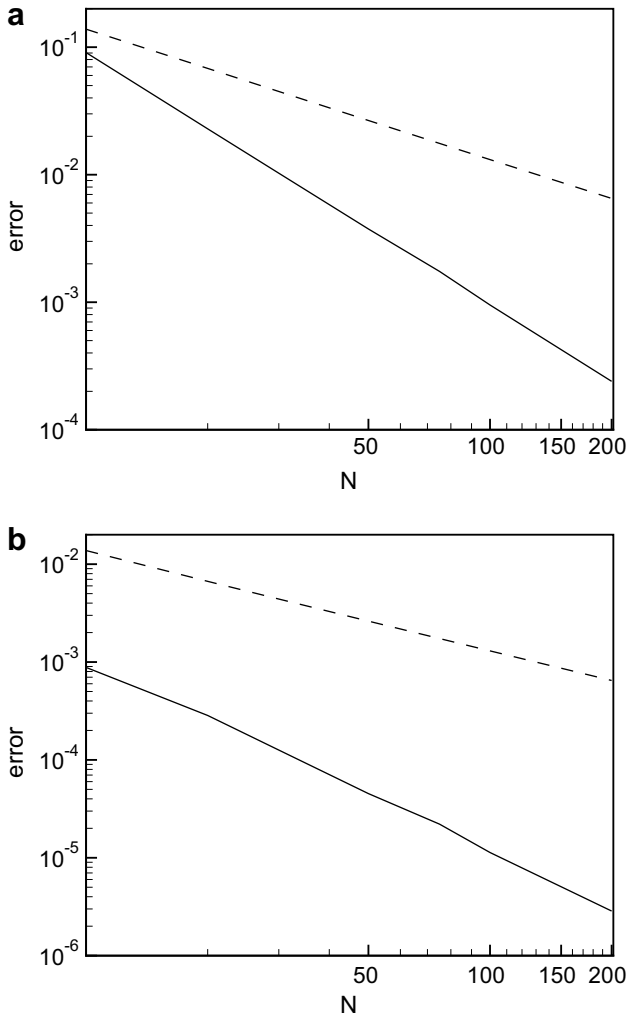


**Fig. 1.** Errors due to the spatial discretization in Couette flow with (a) $Kn = 0.1$ and (b) $Kn = 1$ (dashed line: actual slip velocity $(u_w - u_f)/u_w$, solid line: the slip velocity measured using the velocity gradient at the centerline, $1 - (\mathrm{d}u_x/\mathrm{d}y)|_{y=H/2}/(2U)$, $N$: the number of grid points in the transverse direction).

## 3. Results

### 3.1. Couette flow

In Couette flow, the flow is driven by moving walls. The wall at $y = 0$ moves with a velocity of $-U$, while that at $y = H$ moves with a velocity of $U$. The LB methods are compared with results from DSMC [6] and the linearized Boltzmann equation [44]. The wall velocity $U$ is 0.01 in the lattice unit, while DSMC solutions are obtained for $Ma$ of 0.16. In Willis [44], the solution of the linearized Boltzmann equation is tabulated with the rarefaction parameter $\alpha = H/(\sqrt{2}\tau c_s)$. The rarefaction parameter, $\alpha$, and the viscosity-based Knudsen number are thus related as $Kn = \sqrt{\pi}/(2\alpha)$.

First, the effects of spatial discretization are investigated for a multi-speed LB method where the finite difference method is used for spatial discretization. Fig. 1 shows the spatial discretization errors for D2Q16, for which the analytic solution for Couette flows [31] is known. The error is defined by

$$\epsilon = \frac{|u_{s,a} - u_{s,n}|}{u_{s,a}},$$

where $u_{s,a}$ and $u_{s,n}$ are the slip velocity obtained from the analytic solutions and from the numerical simulations, respectively. For $Kn = 0.1$, the errors for the slip velocity measured using the velocity gradient at the centerline, $1 - (\mathrm{d}u_x/\mathrm{d}y)|_{y=0}/(2U)$, suggest that the present scheme is approximately of second-order. However, the actual slip velocity

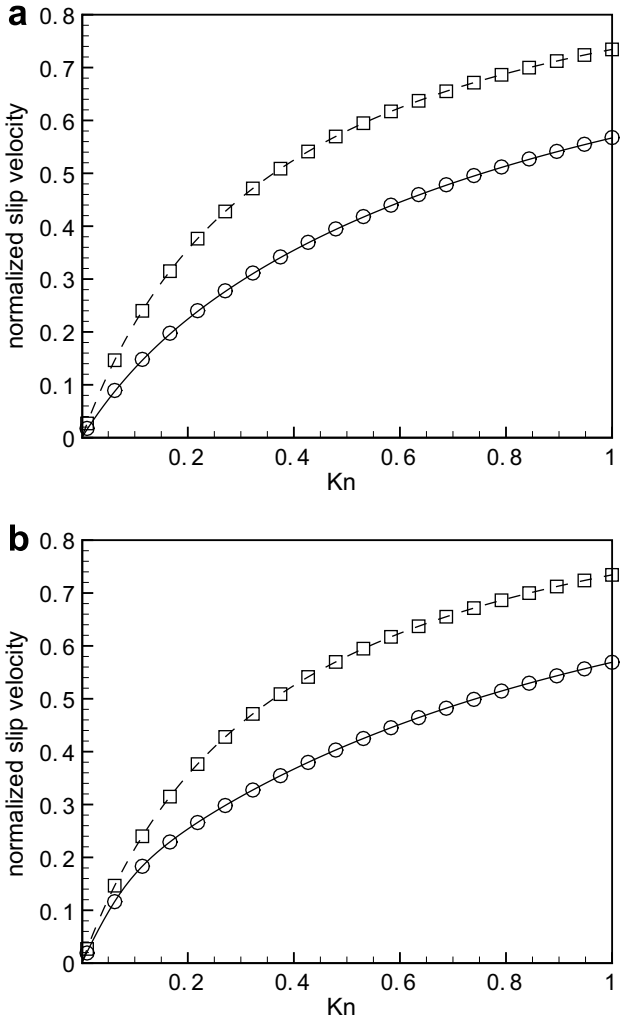


**Fig. 2.** Comparison of the slip velocities from numerical simulations with the analytic solutions in Couette flow. (a) actual slip velocity $(u_w - u_f)/u_w$ and (b) the slip velocity measured using the velocity gradient at the centerline, $1 - (\mathrm{d}u_x/\mathrm{d}y)|_{y=H/2}/(2U)$ (circles: numerical solutions for D2Q16, solid line: analytic solutions for D2Q16, squares: numerical solutions for D2Q9, dashed line: analytic solutions for D2Q9).

at the wall, $(u_w - u_f)/u_w$, is predicted with first-order accuracy, where $u_w$ and $u_f$ are the velocity of the wall and the fluid velocity at the wall, respectively. The same trend is observed for $Kn = 1$, while the errors are much smaller than those for $Kn = 0.1$.

In Fig. 2, the slip velocities from numerical simulations are compared with the analytic solutions for D2Q9 and D2Q16. The transverse direction is discretized into 102 grid points including boundary points. With this fine resolution, numerical solutions are in excellent agreement with analytic solutions. The same grid resolution as in Fig. 2 is used in the following results for Couette and Poiseuille flows.

Before discussing the accuracy of velocity space discretization, the use of second-order equilibrium function in low *Ma*, finite *Kn* flows is justified. In Fig. 3, the slip velocities predicted using first-, second-, and third-order equilibrium functions are shown for D2Q16. The slip velocities predicted using different order of equilibrium functions are almost identical for all *Kn* in Fig. 3. Although the higher-order terms in the equilibrium function are formally required to recover the macroscopic hydrodynamic equation corresponding to the higher-order Chapman–Enskog expansion [26], the higher-order terms in the equilibrium distribution function have negligible influence in flows with very low *Ma*. In steady unidirectional flows investigated here, even first-order equilibrium function (Stokes equilibrium) can be used. For the standard D2Q9 LB method, it can be analytically shown that the slip velocity with the first-order equilibrium function is identical to that with the second-order equilibrium function in steady unidirectional flows [41]. The second-order terms are, however, to be retained in general flows where convection plays a significant role. For higher-order LB methods, the third- and higher-order equilibrium functions are required for Galilean invariance [45,29]. The error for the viscosity due to non-Galilean invariance is $O(Ma^2)$ for the second-order equilibrium function [45] and is, therefore, very small for microscale flows where $Ma \ll 1$.

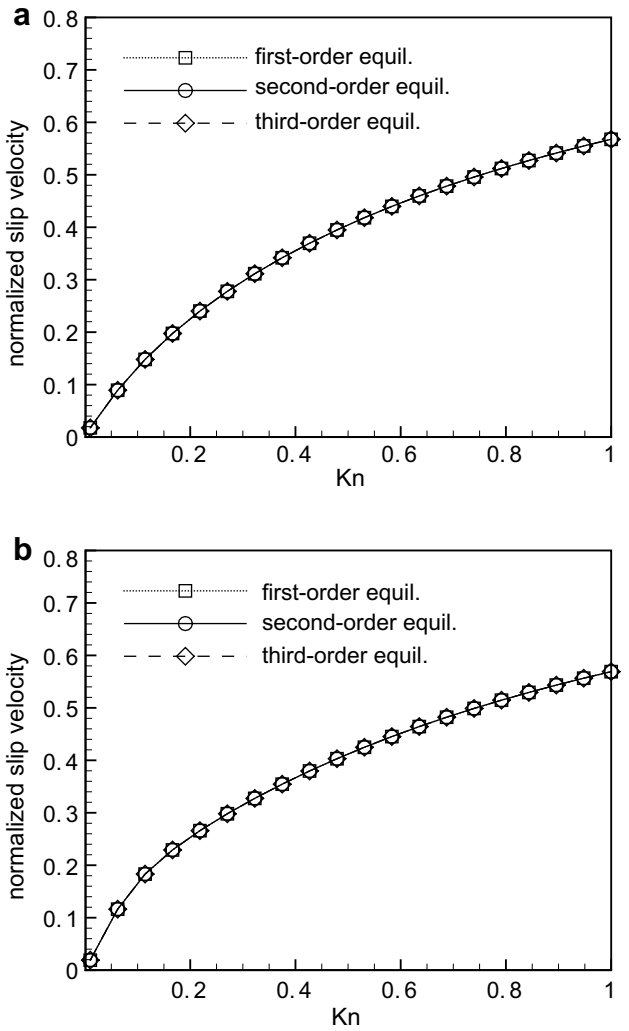


**Fig. 3.** Comparison of the slip velocity predicted using different order of equilibrium functions for D2Q16 in Couette flow. (a) actual slip velocity $(u_w - u_f)/u_w$, and (b) the slip velocity measured using the velocity gradient at the centerline, $1 - (\mathrm{d}u_x/\mathrm{d}y)|_{y=H/2}/(2U)$.

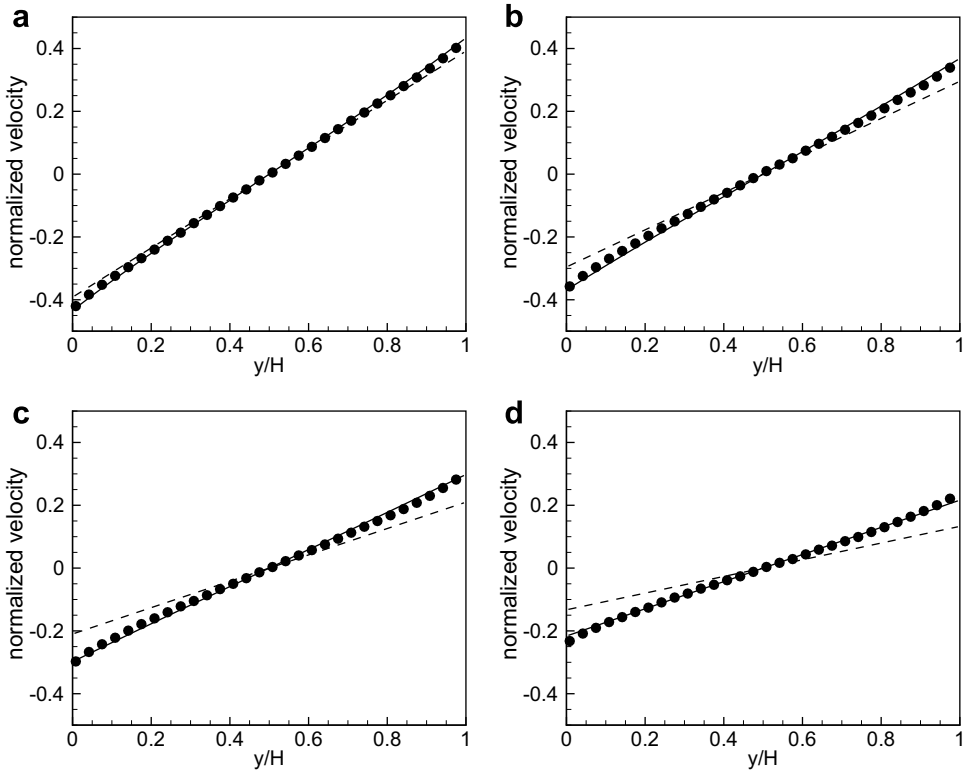


**Fig. 4.** Distribution of streamwise velocity at (a) $Kn = 0.1$, (b) $Kn = 0.25$, (c) $Kn = 0.5$, and (d) $Kn = 1.0$ in Couette flow (symbols: DSMC, solid line: D2Q16, dashed line: D2Q9). The velocity is normalized by the difference of the velocities of the top and bottom plates.

Fig. 4 shows the distribution of the streamwise velocity at $Kn = 0.1$, 0.25, 0.5, and 1. For D2Q9, the departure from DSMC increases as $Kn$ increases. D2Q16 is in excellent agreement with DSMC for all $Kn$ considered here. In DSMC and D2Q16, the nonlinear Knudsen layer is predicted, while D2Q9 gives a linear profile and does not predict the Knudsen layer, as shown in Ansumali et al. [31].

Fig. 5 shows the actual slip velocity at the wall and the slip velocity measured using the velocity gradient at the centerline. The slip velocity based on the velocity gradient outside the Knudsen layer is used for a boundary condition in the macroscopic hydrodynamic equation. In Fig. 5a, the slip velocities predicted by the D2Q16 and D2Q36 schemes are in very good agreement with the solution of the linearized Boltzmann equation for $Kn < 1$. D2Q9 overpredicts the actual slip even at very small $Kn$, while the slip velocity based on the velocity gradient at the centerline is in good agreement with the linearized Boltzmann solution for $Kn < 0.05$. This is because D2Q9 does not capture the Knudsen layer. The D2Q25 scheme also overpredicts the slip velocity, while it gives better results than the D2Q9 scheme. In Fig. 6, the results for the LB schemes with the same order of the Gauss–Hermite quadratures are shown. Even with formally same order of accuracy, the results show strong sensitivity to a quadrature chosen. This can be attributed to the different order of accuracy for high-order off-diagonal moments. While the quadratures with the same order of formal accuracy have the same order of accuracy for the diagonal elements of a moment tensor, the order of accuracy for the off-diagonal moments beyond the formal order of a quadrature can be different for different quadratures.

Fig. 7 shows the normalized shear stress predicted by various LB schemes. The overall trend in accuracy is similar to that for the slip velocity based on the velocity gradient. D2Q9, however, underpredicts the shear stress. For D2Q9, the hydrodynamic equation is exactly the Navier–Stokes equation for all $Kn$, with the viscosity given by $\nu = \tau c_s^2$. The overpredicted slip velocity thus gives the underprediced velocity gradient and shear stress. This behavior is also observed in other LB methods.

All higher-order methods improve the accuracy as compared with the standard LB method. However, the improvement is not monotonic with the order of the Gauss–Hermite quadrature. The hydrodynamic equation for the standard D2Q9 scheme is the isothermal Navier–Stokes equation for the small $Kn$ limit. The next-order LB scheme such as D2Q16 formally corresponds to the thermal Navier–Stokes equation in the Chapmann–Enskog expansion [19]. However, as shown in the analytic solution of Ansumali et al. [31] and the present numerical study for Couette flow, D2Q16 captures the Knudsen layer, while D2Q9 does not. This shows that at finite $Kn$, the hydrodynamic equation for D2Q16 is not just the Navier–Stokes equation. But, as shown in Fig. 8, the difference between the actual slip velocity and the slip velocity based on the velocity gradient outside the Knudsen layer rapidly decreases after $Kn \approx 0.2$, while that predicted by the linearized Boltzmann equation does

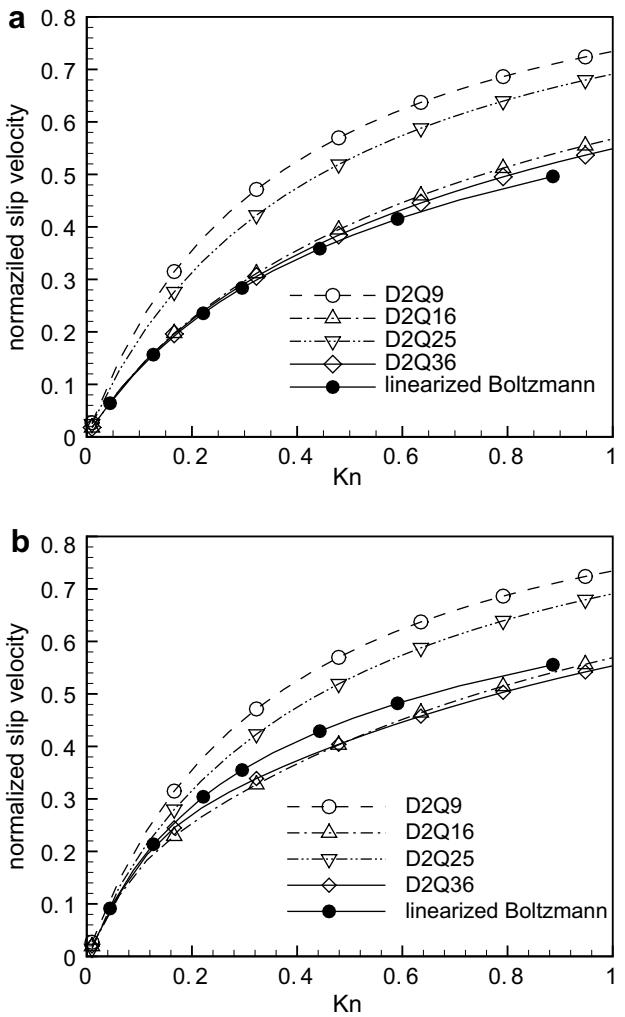


**Fig. 5.** Normalized slip velocity in Couette flow. (a) actual slip velocity $(u_w - u_f)/u_w$, and (b) the slip velocity measured using the velocity gradient at the centerline, $1 - (\mathrm{d}u_x/\mathrm{d}y)|_{y=H/2}/(2U)$.

not. The Knudsen layer disappears at $Kn \approx 0.8$ for D2Q16. D2Q25 performs poorer than D2Q16, although the order of quadrature is higher. For the quadrature with the accuracy one order higher, D2Q36, the Knudsen layer is better predicted than for D2Q16. The slip velocity difference, however, still decreases more rapidly than that for the linearized Boltzmann equation. The Knudsen layer is captured for up to $Kn = \mathrm{O}(0.1)$ by the LB method with up to the 11th order Gauss–Hermite quadrature. This is because the ratio of the smallest (non-trivial) and the largest speeds of the discrete velocities is not sufficiently large in the LB methods studied here. In Kim et al. [41], it is argued that the Knudsen layer cannot be captured by the D2Q9 LB method with single-speed discrete velocities, since the effects of the wall confinement are the same for all particles. In Ansumali et al. [31], it is shown that the lattice constraint on the diagonal elements of the third-order moments is responsible for the lack of the Knudsen layer in D2Q9. For LB methods with multi-speed discrete velocities, when the relaxation time $\tau$ is larger than $\mathrm{O}(H/c_m)$, where $c_m$ is the minimum (non-trivial) speed of particles, all particles do not have sufficient time to equilibrate with the hydrodynamic field before reaching a wall. For sufficiently large $Kn$, the effects of the wall confinement are then similar for all discrete velocities, and the Knudsen layer disappears. To capture the Knudsen layer at $Kn$ larger than $\mathrm{O}(0.1)$, the ratio of the smallest (non-trivial) and the largest speeds of the discrete velocities should be larger than the present ones.

### 3.2. Poiseuille flow

Fig. 9 shows the streamwise velocity for a range of $Kn$. The flow between two parallel plates is driven by a constant pressure gradient, $-g$. At $Kn = 0.04$, D2Q9 and D2Q16 agree well with DSMC, although D2Q9 slightly overpredicts the slip velocity at the wall. While D2Q9 does not perform well for $Kn > 0.1$, D2Q16 remains quantitatively accurate up to $Kn \approx 1$.

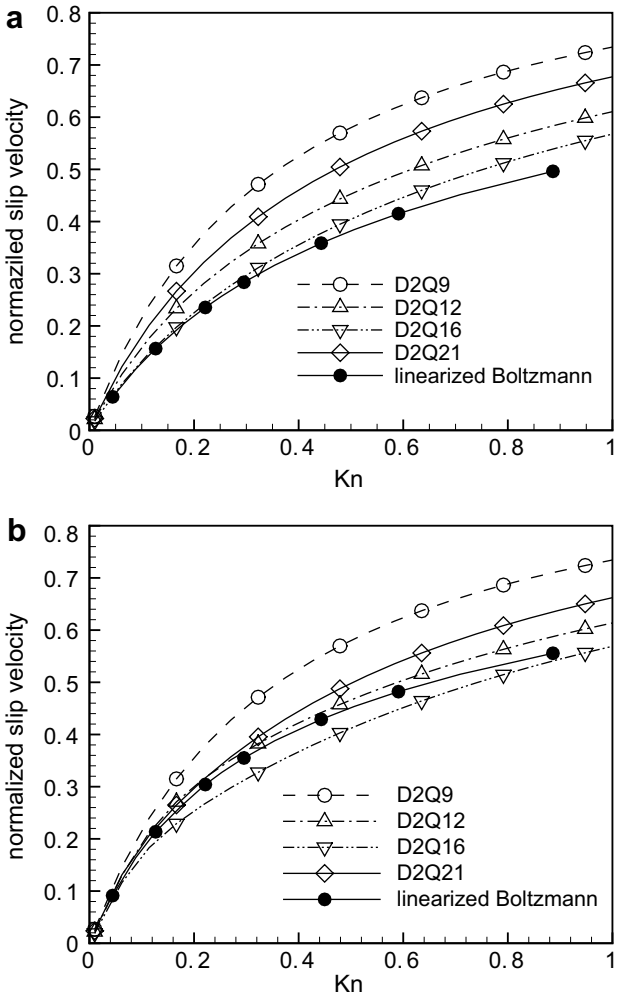


**Fig. 6.** Normalized slip velocity in Couette flow. (a) actual slip velocity $(u_w - u_f)/u_w$, and (b) the slip velocity measured using the velocity gradient at the centerline, $1 - (\mathrm{d}u_x/\mathrm{d}y)|_{y=H/2}/(2U)$. The results for quadratures with the same formal order of accuracy (seventh-order) are shown together with that for the standard D2Q9 quadrature (fifth-order).

However, at $Kn = 1$, the deviation from DSMC is also observed for D2Q16 near the walls. This is because D2Q16 does not capture the Knudsen layer at $Kn \approx 1$.

For Poiseuille flow, a major quantity used in the validation is the normalized mass flux:

$$Q = \frac{1}{4u_0 HKn}\int_0^H u\mathrm{d}y, \tag{38}$$

where $u_0$ is the centerline velocity for the Navier–Stokes equation with no-slip boundary condition, which is given by $u_0 = gH^2/(8\rho\nu)$. For the Navier–Stokes equation with no-slip boundary condition, the normalized mass flow rate $Q$ is given by

$$Q = \frac{1}{6Kn}. \tag{39}$$

In Cercignani et al. [46], the normalized mass flow rate for the linearized Boltzmann equation is obtained using the variational approach. The rarefaction parameter $\delta$ in their study is related to $Kn$ as $\delta = \sqrt{\pi}/(2Kn)$.

In Fig. 10, the normalized mass flow rates predicted by various LB schemes are compared with the linearized Boltzmann equation [46] and DSMC solutions for a range of $Kn$. DSMC solutions agree well with those of the linearized Boltzmann equation, which shows the validity of the linearization of the collision operator in the Boltzmann equation in these low $Ma$ flows. D2Q9 well predicts the mass flow rate up to $Kn \approx 0.1$. All higher-order LB schemes perform better than D2Q9. The D2Q16 scheme agrees well with DSMC and the linearized Boltzmann equation up to $Kn \approx 1$. Note that, as in Couette flow, the accuracy of the LB method does not monotonically increase with the order of the quadrature. While D2Q25 is formally of higher-

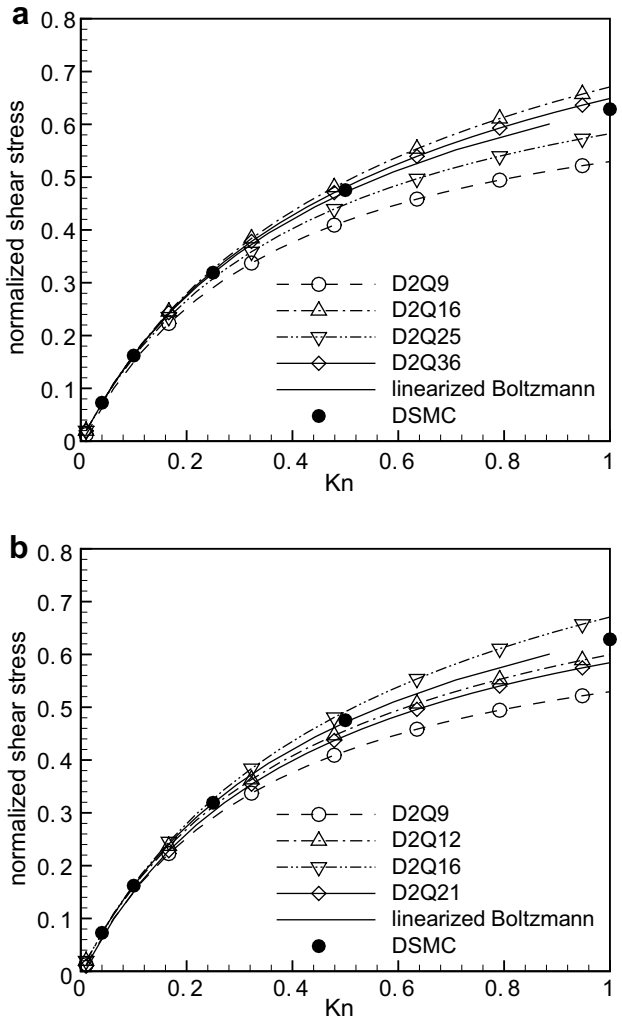


**Fig. 7.** Normalized shear stress. The shear stress is normalized by the asymptotic solution for the free molecular limit, $Kn \to \infty$. In (b), the results for quadratures with the same formal order of accuracy (seventh-order) are shown together with that for the standard D2Q9 quadrature (fifth-order).

order than D2Q16, it does not improve the accuracy. By further increasing the formal order of accuracy, the accuracy of the LB method is improved. The D2Q36 scheme gives the best result among the schemes adopted here. These results are consistent with those for Couette flow. D2Q16 and D2Q36 do not reproduce the Kundsen minimum at $Kn \approx 1$. In Fig. 10b, the normalized mass flow rates predicted by the quadratures with the same order of accuracy are shown. The predictions again show sensitivity to the quadratures.

Cercignani [42] obtained the asymptotic solution for the normalized mass flux for $Kn \ll 1$:

$$Q_\delta = \frac{\delta}{4u_0 H}\int_0^H u dy = \frac{1}{6}\delta + \sigma + \frac{(2\sigma^2 - 1)}{\delta}, \tag{40}$$

where $\sigma = 1.01615$. For consistent comparison with the LB equation, the normalized mass flow rate can be re-written as

$$Q = \frac{1}{6Kn} + c_1 - (2c_2 + c_3)Kn, \tag{41}$$

where $c_1 = 1.1466$, $c_2 = -0.97566$, and $c_3 = 0.59516$. The exact solution for D2Q9 is [41]

$$Q = \frac{1}{Kn} + \sqrt{\frac{6}{\pi}} + \frac{8}{\pi}Kn. \tag{42}$$

The first and second-order slip coefficients are slightly overpredicted by D2Q9. All higher-order LB methods adopted here improve the mass flow rate result.

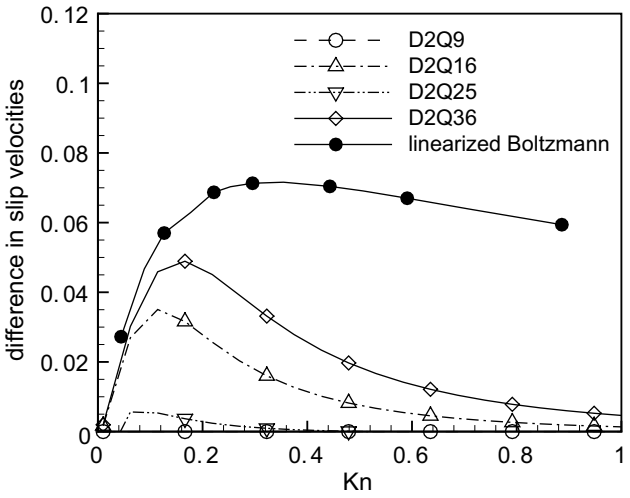


**Fig. 8.** Difference between the actual slip velocity, $(u_w - u_f)/u_w$, and the slip velocity measured using the velocity gradient at the centerline, $1 - (\mathrm{d}u_x/\mathrm{d}y)|_{y=0}/(2U)$, in Couette flow.

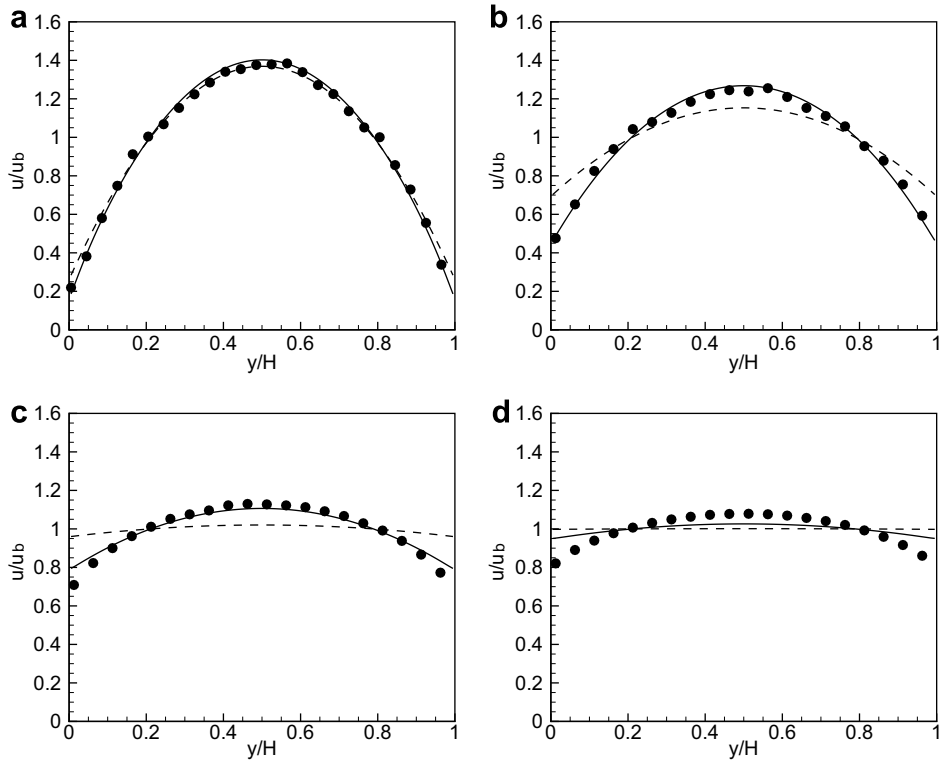


**Fig. 9.** Distribution of streamwise velocity at (a) $Kn = 0.04$, (b) $Kn = 0.2$, (c) $Kn = 1.0$ and (d) $Kn = 5.0$ in Poiseuille flow (symbols: DSMC, solid line: D2Q16, dashed line: D2Q9). The velocity is normalized by $u_b = \int_{-H/2}^{H/2} u\mathrm{d}y/H$.

For large $Kn$, the asymptotic solution for the linearized Boltzmann equation is given by [42]

$$Q \sim \frac{1}{\sqrt{\pi}} \log(Kn). \tag{43}$$

Eqs. (41) and (43) show the presence of the Knudsen minimum [19], which occurs at $Kn \approx 1$ in the linearized Boltzmann equation and DSMC in Fig. 10. For D2Q9, the Knudsen minimum occurs at $Kn = \sqrt{\pi/8}$. For large $Kn$, the mass flow rate predicted by D2Q9 is given by

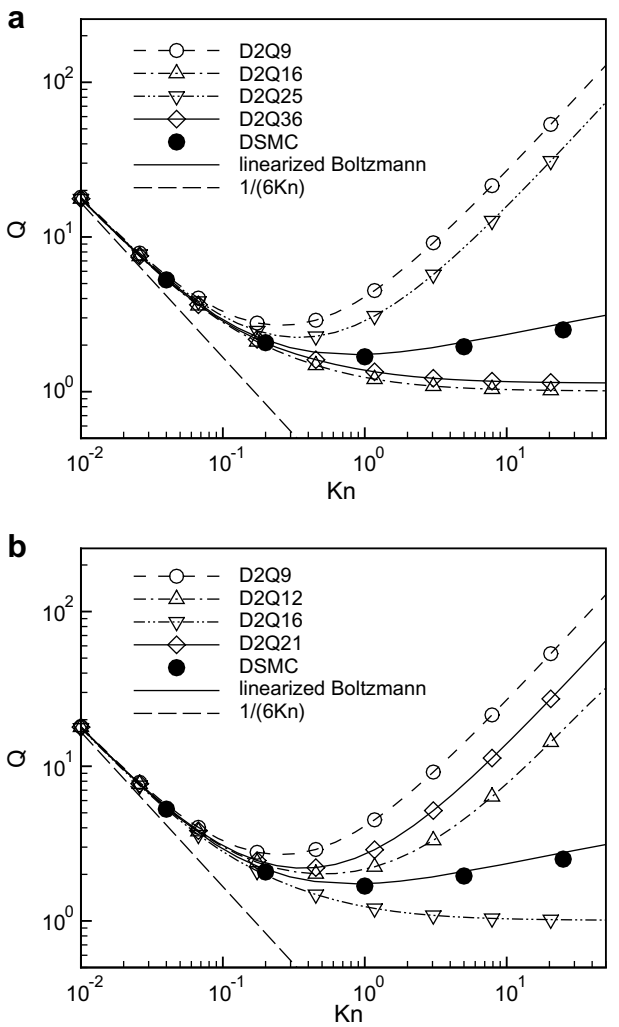


**Fig. 10.** Normalized mass flow rate in Poiseuille flow. In (b), the results for quadratures with the same formal order of accuracy (seventh-order) are shown together with that for the standard D2Q9 quadrature (fifth-order).

$$Q \sim \frac{8}{\pi} Kn. \tag{44}$$

D2Q9 does not capture the slow, logarithmic increase in $Q$ for large $Kn$. D2Q25, D2Q12, and D2Q21 show a behavior similar to D2Q9, $Q \sim Kn$ for large $Kn$. For D2Q16 and D2Q36, $Q$ approaches a constant value $Q_\infty$ when $Kn \to \infty$. The normalized mass flow rates in the large $Kn$ limit, $Q_\infty$, are about 1.009 and 1.132 for D2Q16 and D2Q36, respectively. The Knudsen minimum is not predicted by D2Q16 and D2Q36, and the slip phenomenon is first-order in $Kn$ for D2Q16 and D2Q36 in the large $Kn$ limit. While D2Q16 and D2Q36 predict higher-order slip phenomena for small $Kn$, the higher-order terms vanish at large $Kn$.

## 4. Conclusions

Accuracy of higher-order LB methods is investigated. The velocity space in the higher-order LB methods is represented by up to the eleventh-order Gauss–Hermite quadrature. The diffuse-scattering condition is employed for fluid–wall interactions. Discretization, non-dimensionalization, and the definition of the Knudsen number are discussed in the context of the consistency with the continuum kinetic theory. Detailed comparisons with DSMC and the linearized Boltzmann equation are made for plane Couette and Poiseuille flows.

Results show that all higher-order LB methods adopted here improve the accuracy in finite $Kn$ flows, as compared with the standard LB method. With the consistent definition of $Kn$, the higher-order LB methods are quantitatively accurate up to $Kn = \mathrm{O}(1)$, depending on the quadrature and the type of a flow, while the standard LB method is quantitatively accurate only up to $Kn \approx 0.05$. The improvement in the accuracy is found not to be monotonic with the order of the Gauss–Hermite quad-

rature. The results also show strong sensitivity to the chosen quadrature, even when the Gauss–Hermite quadratures have the same order of formal accuracy. This implies that the accuracy of the higher-order LB methods is determined not only by the order of the quadrature, but also by the quadrature chosen. Among the schemes investigated here, D2Q16 is the most efficient method with good accuracy.

All the higher-order LB methods predict the Knudsen layer. However, due to a finite number of discrete velocities, the Knudsen layer is predicted only for $Kn = \mathrm{O}(0.1)$. The Knudsen layer rapidly disappears when the Knudsen number approaches unity, while it is still present for $Kn = \mathrm{O}(1)$ in the Boltzmann equation. It is also found that the higher-order LB methods adopted here do not capture the asymptotic behavior of the Boltzmann equation for large $Kn$. At large $Kn$, the normalized mass flow rate is either zeroth-order or first-order in $Kn$, while it depends logarithmically on $Kn$ in the Boltzmann equation.

## Acknowledgement

Financial support by Honda R&D Co., Ltd. Fundamental Technology Research Center, is gratefully acknowledged. IDB expresses his gratitude to Stanford University for partial support during a sabbatical leave.

## Appendix

From Eq. (13), we obtain

$$\frac{\partial c_{y,m}\Gamma_m}{\partial y} = -\frac{1}{\tau}(\Gamma_m - \Gamma^{\mathrm{eq}}), \tag{45}$$

where

$$\Gamma_m = \sum_{c_{iy}<0} |c_{iy}| f_i. \tag{46}$$

$$c_{y,m} = \frac{\sum_{c_{iy}<0} c_{iy}|c_{iy}| f_i}{\sum_{c_{iy}<0} |c_{iy}| f_i}, \tag{47}$$

$$\Gamma^{\mathrm{eq}} = \sum_{c_{iy}<0} |c_{iy}| f_i^{\mathrm{eq}} = \sum\nolimits_{c_{iy}>0} |c_{iy}| f_i^{\mathrm{eq}}. \tag{48}$$

Here, $c_{iy} = \mathbf{c}_i \cdot \mathbf{e}_y$. At $y = H$, $\Gamma_m = \Psi_m \Gamma^{\mathrm{eq}}$. The solution for $\Gamma_m$ can be written as

$$\Gamma_m = (\Psi_m - 1)\Gamma^{\mathrm{eq}} \exp\left(-\int_H^y \frac{\mathrm{d}y'}{\tau c_{y,m}}\right) + \Gamma^{\mathrm{eq}}. \tag{49}$$

Similarly, we have

$$\Gamma_p = (\Psi_p - 1)\Gamma^{\mathrm{eq}} \exp\left(-\int_0^y \frac{\mathrm{d}y'}{\tau c_{y,p}}\right) + \Gamma^{\mathrm{eq}}, \tag{50}$$

where

$$\Gamma_p = \sum_{c_{iy}>0} |c_{iy}| f_i. \tag{51}$$

$$c_{y,p} = \frac{\sum_{c_{iy}>0} c_{iy}|c_{iy}| f_i}{\sum_{c_{iy}>0} |c_{iy}| f_i}. \tag{52}$$

From Eqs. (49) and (50), we obtain

$$\rho u_y = \Gamma_p - \Gamma_m = (\Psi_p - 1)\Gamma^{\mathrm{eq}} \exp\left(-\int_0^y \frac{\mathrm{d}y'}{\tau c_{y,p}}\right) - (\Psi_m - 1)\Gamma^{\mathrm{eq}} \exp\left(-\int_H^y \frac{\mathrm{d}y'}{\tau c_{y,m}}\right). \tag{53}$$

Since $u_y = 0$ for all $y$, we have $\Psi_m = \Psi_p = 1$.

## References

[1] C.-M. Ho, Y.-C. Tai, Micro-electro-mechanical-systems (MEMS) and fluid flows, Annu. Rev. Fluid Mech. 30 (1998) 579–612.
[2] N.G. Hadjiconstantinou, The limits of Navier–Stokes theory and kinetic extensions for describing small-scale gaseous hydrodynamics, Phys. Fluids 18 (2006) 111301.
[3] M. Knudsen, Die gesetze der molecular stromung und dieinneren reibungstromung der gase durch rohren, Annu. Phys. 28 (1909) 75.
[4] S. Chapman, T.G. Cowling, The Mathematical Theory of Non-uniform Gases, Cambridge University Press, Cambridge, 1970.
[5] C. Cercignani, The Boltzmann Equation and Its Applications, Springer-Verlag, New York, 1988.
[6] G.A. Bird, Molecular Gas Dynamics and the Direct Simulation of Gas Flows, Oxford University Press, Oxford, 1994.
[7] W. Wagner, A convergence proof for Bird's direct simulation Monte Carlo method for the Boltzmann equation, J. Stat. Phys. 66 (1992) 1011–1044.

[8] G.R. McNamara, G. Zanetti, Use of the Boltzmann equation to simulate lattice-gas automata, Phys. Rev. Lett. 61 (1988) 2332.
[9] Y.H. Qian, D. d'Humières, P. Lallemand, Lattice BGK models for Navier–Stokes equation, Europhys. Lett. 17 (1992) 479–484.
[10] S. Chen, G.D. Doolen, Lattice Boltzmann method for fluid flows, Annu. Rev. Fluid Mech. 30 (1998) 329–364.
[11] R. Benzi, S. Succi, M. Vergassola, Thee lattice Boltzmann-equation – Theory and applications, Phys. Reports 222 (1992) 145–197.
[12] S. Succi, The Lattice Boltzmann Equation for Fluid Dynamics and Beyond, Oxford University Press, Oxford, 2001.
[13] X. He, L.S. Luo, A priori derivation of the lattice Boltzmann equation, Phys. Rev. E 55 (1997) R6333.
[14] X. Shan, X. He, Discretization of the velocity space in the solution of the Boltzmann equation, Phys. Rev. Lett. 80 (1998) 65.
[15] X.B. Nie, G.D. Doolen, S.Y. Chen, Micro-electro-mechanical-systems (MEMS) and fluid flows, J. Stat. Phys. 107 (2002) 279–289.
[16] C.Y. Lim, C. Shu, X.D. Niu, Y.T. Chew, Application of lattice Boltzmann method to simulate microchannel flows, Phys. Fluids 14 (2002) 2299–2308.
[17] S. Ansumali, I.V. Karlin, Kinetic boundary condition in the lattice Boltzmann method, Phys. Rev. E 66 (2002) 026311.
[18] F. Toschi, S. Succi, Lattice Boltzmann method at finite Knudsen numbers, Europhys. Lett. 69 (2005) 549–555.
[19] S. Ansumali, I.V. Karlin, C.E. Frouzakis, K.B. Boulouchos, Entropic lattice Boltzmann method for microflows, Physica A 359 (2006) 289–305.
[20] T. Lee, C.L. Lin, Rarefaction and compressibility effects of the lattice-Boltzmann-equation method in a gas microchannel, Phys. Rev. E 71 (2005) 046706.
[21] V. Sofonea, R.F. Sekerka, Boundary conditions for the upwind finite difference lattice Boltzmann model: Evidence of slip velocity in micro-channel flow, J. Comp. Phys. 207 (2005) 639–659.
[22] R. Zhang, X. Shan, H. Chen, Efficient kinetic method for fluid simulation beyond Navier–Stokes equation, Phys. Rev. E 74 (2006) 046703.
[23] B. Li, D.Y. Kwok, Discrete Boltzmann equation for microfluidics, Phys. Rev. Lett. 90 (2003) 124502.
[24] L.-S. Luo, Comment on Discrete Boltzmann equation for microfluidics, Phys. Rev. Lett. 92 (2004) 139401.
[25] Z. Guo, T.S. Zhao, Y. Shi, Physical symmetry, spatial accuracy, and relaxation time of the lattice Boltzmann equation for microgas flows, J. Appl. Phys. 99 (2006) 074903.
[26] X. Shan, X.-F. Yuan, H. Chen, Kinetic theory representation of hydrodynamics: a way beyond Navier–Stokes equation, J. Fluid Mech. 550 (2006) 413–441.
[27] S. Ansumali, I.V. Karlin, H.C. Ottinger, Minimal entropic kinetic models for hydrodynamics, Europhys. Lett. 63 (2003) 798–804.
[28] S.S. Chikatamarla, S. Ansumali, I.V. Karlin, Entropic lattice Boltzmann models for hydrodynamics in three dimensions, Phys. Rev. Lett. 97 (2006) 010201.
[29] S.S. Chikatamarla, I.V. Karlin, Entropy and Galilean invariance of lattice Boltzmann theories, Phys. Rev. Lett. 97 (2006) 190601.
[30] P.C. Philippi, L.A. Hegele, L.O.E. dos Santos, R. Surmas, From the continuous to the lattice Boltzmann equation: The discretization problem and thermal models, Phys. Rev. E 73 (2006) 056702.
[31] S. Ansumali, I.V. Karlin, S. Arcidiacono, A. Abbas, N.I. Prasianakis, Hydrodynamics beyond Navier–Stokes: Exact solution to the lattice Boltzmann hierarchy, Phys. Rev. Lett. 98 (2007) 124502.
[32] A.H. Stroud, Approximate calculation of multiple integrals, Prentice-Hall, Inc., 1971.
[33] X. He, X. Shan, G. Doolen, Discrete Boltzmann equation model for nonideal gases, Phys. Rev. E 57 (1998) R13–R16.
[34] R. Mei, W. Shyy, On the finite difference-based lattice Boltzmann method in curvilinear coordinates, J. Comp. Phys. 143 (1998) 426–448.
[35] B. van Leer, Towards the ultimate conservative difference scheme. v. a second-order sequel to Godunov's method, J. Comp. Phys. 32 (1979) 101–136.
[36] A. Bardow, I.V. Karlin, A.A. Gusev, General characteristic-based algorithm for off-lattice Boltzmann simulations, Europhys. Lett. 75 (3) (2006) 434–440.
[37] A. Bardow, I.V. Karlin, A.A. Gusev, Multispeed models in off-lattice Boltzmann simulations, Phys. Rev. E 77 (2008) 025701.
[38] Y.-H. Zhang, X.J. Gu, R.W. Barber, D.R. Emerson, Capturing Knudsen layer phenomena using a lattice Boltzmann model, Phys. Rev. E 74 (2006) 046704.
[39] V. Sofonea, R.F. Sekerka, Diffuse-reflection boundary conditions for a thermal lattice Boltzmann model in two dimensions: Evidence of temperature jump and slip velocity in microchannels, Phys. Rev. E 71 (2005) 066709.
[40] C. Cercignani, Slow Rarefied Flows, Birkhäuser Basel, 2006.
[41] S.H. Kim, H. Pitsch, I.D. Boyd, Slip velocity and Knudsen layer in the lattice Bolzmann model for microscale flows, Phys. Rev. E 77 (2008) 026704.
[42] C. Cercignani, Theory and application of the Boltzmann equation, Academic Press, 1975.
[43] M. Sbragaglia, S. Succi, Analytic calculation of slip flow in lattice Boltzmann models with kinetic boundary conditions, Phys. Fluids 17 (2005) 093602.
[44] D.R. Willis, Comparison of kineric theory analyses of linearized couette flow, Phys. Fluids 5 (1962) 127–135.
[45] Y.-H. Qian, Y. Zhou, Complete Galilean-invariant lattice BGK models for the Navier–Stokes equation, Europhys. Lett. 42 (4) (2006) 359–364.
[46] C. Cercignani, M. Lampis, S. Lorenzani, Variational approach to gas flows in microchannles, Phys. Fluids 16 (2004) 3426–3437.